



Flow Estimation by Flow Induced Vibration of Bluff Bodies

A. Tamil Chandran^{1†}, T. Suthakar², K. R. Balasubramanian² and S. Rammohan¹

¹ Fluid Control Research Institute, Palakkad, Kerala- 678623, India

² Department of Mechanical Engineering, National Institute of Technology- Trichirapallai, Tamil Nadu, India

†Corresponding Author Email: tamilchandran@fcriindia.com

(Received January 14, 2022; accepted May 30, 2022)

ABSTRACT

The study confirms the feasibility of using information from flow-induced vibration generated by bluff bodies for measurement of flow. The proposed methodology is based on experiments conducted for recording acceleration signals from vibration sensors embedded along with bluff bodies in cross flow. The studies were undertaken in a wide Reynolds number range of 4700 to 5.655×10^5 , with five different geometries of bluff bodies for shape optimization. Resonance and vortex shedding frequencies of samples are determined experimentally. The recorded acceleration signals are analysed using three different techniques such as frequency shift method, resonance amplitude method and overall acceleration estimation method. In this, the frequency shift method shows correlation at low flow velocities. In the resonance amplitude method and overall acceleration method, acceleration levels show a cubic relation with the flow rate. In the resonance amplitude method, obtained R^2 values are from 0.93 to 0.99. Overall acceleration estimation method has shown better correlation with flow rate and its R^2 values were above 0.99. The study confirms that application of all three methods together yields reasonably good estimation for a wide range of flow.

Keywords: Flow measurement; Vibration measurement; Cross flow; Overall amplitude method; Resonance frequency.

NOMENCLATURE

D_{ff}	frictional drag force	ρ	fluid density
D_{pf}	pressure drag force	p	fluid pressure
u	free stream velocity	D_{sf}	static drag force
C_{df}	frictional drag coefficient	D_{df}	dynamic drag force
C_{dp}	pressure drag coefficient	p_t	total pressure
'A'	frontal area	p_s	static pressure
\bar{u}	time averaged velocity	'q'	distributed load
u'	fluctuation velocity	E	Young's modulus
p_d	dynamic pressure	I	moment of inertia
M	bending moment	x, y	co-ordinates
S	Strouhal number	f_n	natural frequency
V_r	reduced velocity	f_s	Strouhal frequency

1 INTRODUCTION

Quantification of an item consumed or transferred is essential in various aspects. Engineering plays a major role in accuracy and the easiest way of quantification. Quantification of oil, gas, water, etc transferred/ consumed by a consumer and sewage discharge by various parties are essential for proper

accountability. Flow meter is an equipment used to quantify the flow transferred. Flow meters are classified based on flow medium and flowing channel. Boiten (1993), has discussed in detail about various flow measurement instruments. Flow meters are developed based on various techniques such as

pressure difference across the flow element and velocity of flowing fluid. In pressure difference technique, the pressure drop developed by the flow element is square of the flow passing through it. It has been documented by [Chattopadhyay \(2006\)](#).

In addition to the differential pressure and velocity measurement method, some of the recently developed flow meters are working based on techniques such as Coriolis Effect of the flow passing through the tube, effect of flow velocity on ultrasonic sound waves and Electro Magnetic Effect (EMF) of flow velocity. Flow meters developed based on the above effect are known as Coriolis Mass flow meter, Ultrasonic flow meter and Electro Magnetic Flow meter respectively. In recent times researches are focused on developing new technology for flow measurement. [Osman *et al.* \(2018\)](#) has studied the feasibility of using various techniques such as direct cross correlation technique, continuous wavelet transform technique and Fast Fourier Technique for flow measurement. Based on the requirement of having a cost effective flow meter with ease of installation and with better accuracy for challenging environments such as large ducts with various shapes, it is focused to develop a flow measurement technique.

In this, studies are conducted with a vibration sensor attached on a cantilever bluff body and by measuring the Flow Induced Vibration (FIV) generated by the flow. This was based on the studies conducted by [Pittard and Blotte \(2003\)](#) about the dynamic pressure fluctuation in the fluid by using the Reynolds – averaged Navier- Stokes (RANS) method and Large Eddy Simulation (LES) method. [Evans *et al.* \(2004\)](#) has extended the work of [Pittard \(2003\)](#) and experimentally demonstrated. From the experiments conducted it was documented that the standard deviation of vibration parameter generated by the flow is proportional to the flow passing through the pipe. [Evans *et al.* \(2004\)](#) have proved the work of [Pittard \(2003\)](#) by experiments. [Medeiros *et al.* \(2015\)](#) extended the work done by [Evans *et al.* \(2004\)](#), and proved that the FIV is proportional to the flow passing through the pipe. In order to increase the accuracy of measurement, in addition to fluid flow [Kim and Kim \(1996\)](#), has used an external source for excitation. [Gama *et al.* \(2009\)](#) have studied with ‘U’ type bends to increase the vibration levels and observed an improvement between the FIV and flow rate. [Riverin and Pettigrew \(2007\)](#) studied the vibration levels generated by flow in a U type bend and reported the results as a spectrum for the studied flow rate range. Based on the reviews conducted, experiments were initiated on bluff bodies to correlate the FIV and flow rate passing through the pipe.

Details discussed in this paper are as follows. Theoretical overview for vibration based flow sensor is discussed in section 2 and experimental facility and sample details are discussed in section 3. Details of the data acquisition system used are discussed in section 4 and results are presented and discussed in section 5. Conclusion of the experimental studies are as given in section 6.

2 THEORETICAL OVERVIEW

In this section, flow induced vibration in cross flow and effect of vortex induced vibration in bluff bodies are discussed.

2.1 Flow Induced Vibration

When the bluff body is in cross flow, it will be subjected to forces due to static pressure, dynamic pressure and shear effect. The sum of all the components of forces in the direction of flow is called drag force. Friction drag is created by shear stress acting on the body. On the other hand, pressure drag is due to the pressure force in the flow direction. It is also known as form drag. Pressure/form drag strongly depends on the shape or form of the object. Friction drag acting on the flat plates having a frontal area 'A', oriented parallel to upstream flow is given by the expression by [Lauder and Spalding \(1974\)](#) as given in Eq. (1) and pressure drag is as given in Eq. (2)

$$D_{ff} = C_{df} \frac{1}{2} \rho A u^2 \quad (1)$$

$$D_{pf} = C_{dp} \frac{1}{2} \rho A u^2 \quad (2)$$

Where u - is flow velocity

Combined drag force is, addition of both the forces and is given in Eq. (3)

$$D_f = D_{pf} + D_{ff} \quad (3)$$

From Eq. (1) and (2) it is observed that, in addition to the free stream velocity, drag coefficient plays a major role in the force generated on the bluff body. To derive a drag coefficient for various shapes, numerous experimental studies and numerical works were conducted on various shapes. It has been well documented by [Belvins \(1984\)](#). [Tamil Chandran *et al.* \(2022\)](#) determined the drag coefficient of various geometries by using a turbulence model. It was done for the three-dimensional geometry by numerical prediction. Drag coefficient varies with Reynold’s number and the time scale of turbulence. Vortex shedding and turbulence act as a source for vibration excitation. Effect of vortex shedding plays a major role in vibration excitation. Vortex shedding frequency is the source for lock-in phenomena and it will occur when it coincides with the system’s natural frequency. Turbulence excitation will be present in the turbulent flow region. The effect of turbulence in time scale plays a major role in dynamic excitation and hence the drag coefficient.

In turbulent flow, total flow velocity at a point is a superposition of instantaneous fluctuating velocity and average velocity at that point. The instantaneous velocity is as given in Eq. (4)

$$u = \bar{u} + u' \quad (4)$$

where, \bar{u} - mean velocity

u' – Fluctuating velocity

As the fluid approaches the bluff body, it has kinetic energy. Due to sudden stoppage of flowing fluid, it will be converted into pressure. The pressure fluctuation induced by the turbulent flow acts as a

dynamic force on the bluff body, which acts as an excitation source for the FIV.

Using Newton's laws of motion, one dimensional fluid flow equation for inviscid fluid is given in Eq. (5) (see [White and Frank, 2016](#)).

$$\rho u \frac{du}{dx} = -\frac{dp}{dx} \quad (5)$$

Where ρ – fluid density, p – fluid pressure

By manipulating the above equation we get the Eq. (6)

$$p_s + \frac{\rho u^2}{2} = \text{constant} = p_t \quad (6)$$

Where

p_s – static pressure

p_t – total pressure

$$\frac{\rho u^2}{2} - \text{dynamic pressure } (p_d)$$

Pressure acting on the bluff body will create force on it. It depends on the differential pressure acting on the front and back side of the bluff body. It is reported that the pressure distribution on the front side is quite stable for a wide range of Reynolds numbers by [Xinliang *et al.* \(2014\)](#). So the force is mainly dominated by the pressure acting on the rear side of the bluff body. As in Eq. (2), drag force per unit area of the bluff body is proportional to density of fluid, drag coefficient and square of the free stream velocity. Various researchers documented that the drag coefficient in turbulent flow is dynamic in nature and is proportional to the flow velocity and it creates dynamic drag on the bluff body. This dynamic (time varying) drag coefficient contributes to the dynamic part of the force acting on the bluff body. As discussed by [Tamil Chandran *et al.* \(2022\)](#), except at very low flows, contribution of frictional drag to the drag coefficient is only 2% to 3% of the pressure drag acting on it. So, by neglecting the frictional component, the drag force Eq. (3), can be rewritten as a combination of static and dynamic drag forces. It is as given in Eq. (7).

$$D_f = D_{sf} + D_{df} \quad (7)$$

Where

D_{sf} – Static drag force, D_{df} – Dynamic drag force

In structural analysis, differentiating the bending moment equation for the beam as given by [De Silva \(2006\)](#) is in Eq. (8).

$$\frac{d^2M}{dx^2} = EI \frac{d^4y}{dx^4} \quad (8)$$

The Euler–Bernoulli equation for relationship between the beam's deflection and the applied load and is as given in Eq. (9)

$$EI \frac{d^4y}{dx^4} = q \quad (9)$$

When the bluff body is in flow path, both static and dynamic drag force act on it. Since the static drag force can only make structural deformation, the dynamic drag force acts as an excitation source. So

by omitting the static drag force, with the dynamic drag force Eq. (9) becomes

$$EI \frac{d^4y}{dx^4} = D_{df} \quad (10)$$

From Eq. (8) and (10) we get the structural and fluid flow relation as given in Eq. (11).

$$\frac{d^2M}{dx^2} = EI \frac{d^4y}{dx^4} = D_{df} \quad (11)$$

Governing equation for the beam is obtained as below.

Euler-Bernoulli equation for beam bending reported by [De Silva \(2006\)](#)

$$EI \frac{\partial^4y}{\partial x^4} + \rho A \frac{\partial^2y}{\partial t^2} = f(x, t) \quad (12)$$

For the free vibration case, i.e. $f(x,t)=0$, the equation of motion Eq.(12) becomes

$$EI \frac{\partial^4y}{\partial x^4} + \rho A \frac{\partial^2y}{\partial t^2} = 0 \quad (13)$$

Where, $\frac{\partial^2y}{\partial t^2}$ is the local acceleration

From Eq. (11) and (13), we can get the correlation between the acceleration and drag force acting on the structure. It can be written as in Eq. (14)

$$\frac{\partial^2y}{\partial t^2} = \frac{D_{df}}{\rho A} \quad (14)$$

From Eq. (14), it is observed that the acceleration generated by the drag force on the bluff body is proportional.

This is the origin for the study of the relation between the drag force acting on a bluff body and FIV generated.

2.2 Vortex-Induced Vibration

When a bluff body is in cross flow, due to flowing fluid, alternately shedding vortices will occur on both sides of it. Vibration induced by this shedding is known as Vortex-Induced Vibration (VIV). This excitation frequency is proportional to the velocity of flowing fluid. When it reaches the natural frequency of the bluff body, large vibration amplitudes will be observed in the bluff body and further increase in flow velocity, there will not be a change in the excitation frequency. This region is known as the lock-in region. This will be represented with reduced velocity in 'x – axis' and amplitude in 'y-axis'. Reduced velocity is a ratio between free stream velocity of flowing fluid and natural frequency of bluff body multiplied with its diameter as given in Eq. (15)

$$\text{Reduced velocity } V_r = \frac{U}{f_n D} \quad (15)$$

When the reduced velocity reaches the critical value, the bluff body will become unstable. The region up to it reaching the critical value is known as the initial branch and after the critical point is known as the lower branch. [Manzoor *et al.* \(2012\)](#) has identified the critical frequency of a square cylinder as 10. Up to the critical point, the vibration amplitude was increasing gradually and from the critical point it was

gradually reducing with minimum amplitude at the reduced frequency of 14. [Chen *et al.* \(2022\)](#) reported that the critical point for cylindrical shape is 4.

The critical point is based on the geometrical shape and it can be defined based on the Strouhal number and drag coefficient of the bluff body. Strouhal number varies based on the geometry. [Belvins \(1984\)](#) documented the Strouhal number of various geometries and found that it varied from 0.12 to 0.28. [Hoerner \(1965\)](#) proposed a relationship between drag coefficient and Strouhal number and it is given in Eq. (16).

$$S = \frac{0.21}{c_d^{3/4}} \quad (16)$$

With the above equation, the Strouhal number for the various shapes used in this study can be determined. Strouhal frequency for each bluff body can be determined by using the Eq. (17).

$$f_s = \frac{SV}{D} \quad (17)$$

3. EXPERIMENTAL TEST FACILITY

In this section, facilities used for simulating the required flow conditions and instruments used for this study are discussed. In addition to the experimental facility, details of test specimens used were also discussed in detail.

3.1 Flow Facility

Flow facility used consists of a pump, constant head tank, test section, flow meters and set of valves. Using this facility, a maximum nominal pipe size of up to 150 mm can be used with a flow rate of up to 300 m³/h. System overall uncertainty of flow measurement is 0.4%. A schematic of the loop is as shown in Fig. 1. Photograph of the test facility is as in Fig. 2.

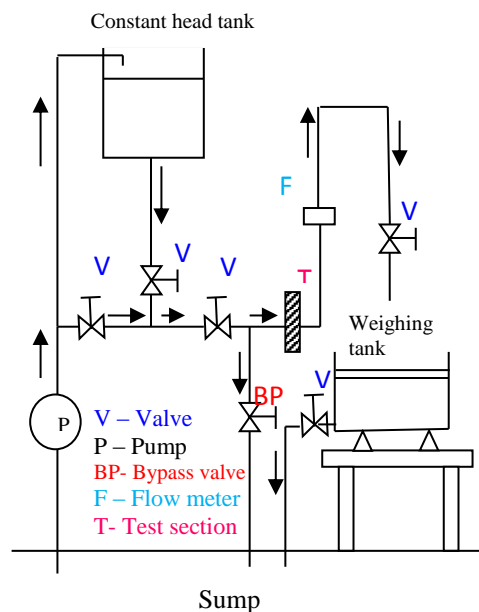


Fig. 1. Schematic of gravity driven test setup.



Fig. 2. Test set up – photograph

For direct pumping, setoff centrifugal pumps are available and they are operated by variable-speed drives. For achieving the desired flow rates the variable speed drives can be adjusted. The bypass loop available in the test loop provides an alternate path for controlling the flow through the test loop.

In this testing, a gravity driven method is used. In gravity driven mode, the water from the sump is directly pumped into the overhead tank and the water level in the tank is maintained by providing control/overflow devices. During measurement, the fluid is directly sent to the test section by gravity mode and the flow is controlled by the control valve installed downstream of the flow loop. To avoid the pipe running in a partially filled condition, the downstream side of the test loop is connected with a bend pipe, having sufficient height. Two different sizes of valves are available to control the flow, with which fine control in the flow can be achieved. Since in gravity driven mode there will not be any external vibration, it is used for this study. The test samples were connected to the flow loop, between two flanges of the test loop. In between the flanges and the test specimen, standard gaskets are used to avoid the leak of fluid.

3.2 Test Instrumentation

The test instrumentation consists of an Electro Magnetic Flow meter (EMF) and vibration measurement system. EMF is used to quantify the flow passing through the test system and a vibration measurement instrument is used to record the FIV generated by turbulent flow on the bluff body. Details about the instrumentation used are as discussed in sections 3.2.1 and 3.2.2.

3.2.1 Flow measurement device

For quantifying the flow that passes through the flow loop, EMF is installed on the upstream side of the test specimen. Since the EMF is a full bore type, it offers minimum resistance in the flow line with no moving parts. It can be used for a wide range of applications and it is well suited for reference applications. Electromotive force produced in this type of flow meters is proportional to the flow velocity passing through it. Nominal diameter of the flow meter is determined based on the diameter of the pipe and the flow rate to be measured. The optimum velocity of flow suggested by the manufacturer is between 2 m/s and 3 m/s. Based on

their recommendation and to meet the wide velocity range, three different sizes i.e., flow meter having nominal diameter of 15mm, 50mm and 150 mm are selected. Each flow meter can be used in the wide velocity range of 0.3 m³/h to 9 m³/h. Make of the flow meter is Endress+Hauser and the model is Promag 50 P 1/2", Promag 50 P 2" and Promag 50 W 6" respectively. During the study, a suitable flow meter was selected based on the flow velocity requirement. Flow meters used are calibrated by using the first principle method (weighing method). With this the uncertainty of 0.4% is achieved in flow measurement.

3.2.2 Vibration measurement system

Vibration measurement system consists of a vibration sensor, signal conditioner and a vibration analyzer. Vibration sensor used is an underwater type accelerometer of model AP 78 and make by M/s AP Technologies, USA. It can use up to 50 meter of water column. It is a charge type sensor having nominal sensitivity of 10 pC/g. It can be used for a wide frequency range from 0.5 Hz to 15000 Hz. For converting the charge output of the accelerometer to voltage, a signal conditioner of model M72B3 of make M/s MMF, Germany is used. It has a gain setting of 0.1, 1, 10, 100 & 1000 mV/pC with accuracy in measurement of ± 0.5 % of the measured value. It has a low pass filter of 100, 1000, 10000 & 50000 Hz and a high pass filter of 3 Hz. Crystal Instruments make CoCo-80 data acquisition systems used for recording the vibration data. It has a band width of 40 kHz, 24 bit with dynamic range of 150 dB. It can take various inputs such as Voltage, ICP/IEPE etc with a maximum range of ±10 V. Combined uncertainty of the vibration measurement system is 1.8%.

3.3 Test Specimen

For this study, a flow loop having a diameter of 150 mm is used. In this, the test section consists of a flange and various cross sections of bluff bodies are used and are connected in between the flanges of the test loop. The bluff body is made up of SS304 stainless steel beam and is attached with a standard 6 inch 150 class flange.

Five different geometries used are as in Fig. 3. The samples are identified with sample no. and are as given in Table 1. Line sketch of the sample with the measurement sensor is as in Fig. 4. Length of the bluff body 'l' considered was 110 mm and it is passing well beyond the center of the flow path and its width 'w' is 10 mm. It was considered based on the length optimization study conducted and reported by Tamil Chandran *et al.* (2020). Blockage ratio of the sample used is 6.2 %. Vibration sensor was connected at the tip of the bluff body to avoid any miss out of the response of first and second natural frequency and to get maximum amplitude. The sensor was mounted on the back side of the bluff body, to avoid any direct force acting on the sensor due to fluid flow. It was mounted using screws, so that it will always get a positive attachment to the bluff body. It is mounted in the flow direction to sense the vibration in that direction.

Table 1 Sample identification

Sample no. as on Fig. 3	Sample no.	Geometry
a	1	Rectangle (beam/plate)
c	2	Semicircular (Semi Cylinder)
d	3	Circular (Cylinder)
b	4	Triangle (Triangular prism)
e	5	Triangle with semicircular front

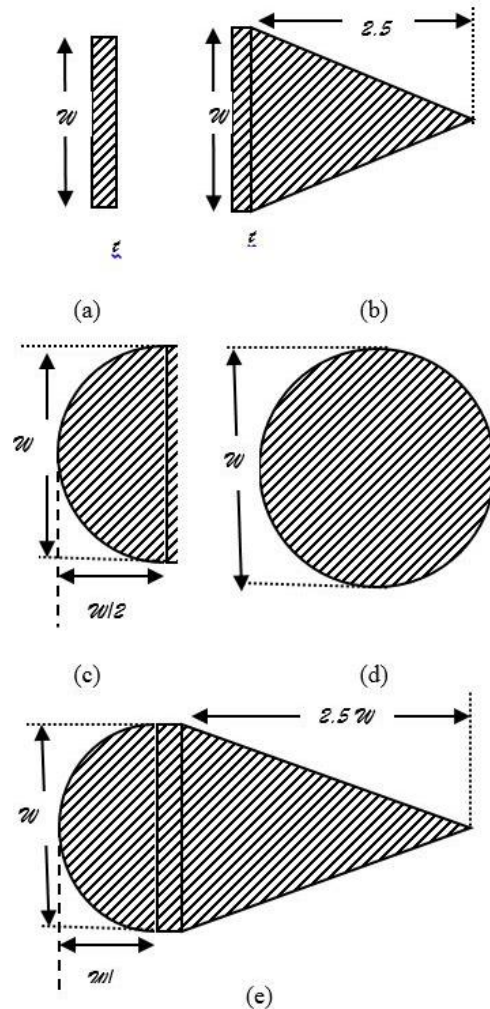


Fig. 3. Geometrical shapes : (a) Plate/ Beam, (b) Triangle (Triangular prism), (c) Semi-circle, d) Circular (cylinder) and (e) Triangle with semicircular front.

4 DATA ACQUISITION SYSTEM

The schematic of the data acquisition system discussed in section 3 is as shown in Fig. 5. The accelerometer used for sensing the vibration is capable of sensing up to the frequency range of 15000 Hz. For measuring the FIV signal. Evans *et al.* (2004) used the sampling rate of 2048 samples/sec

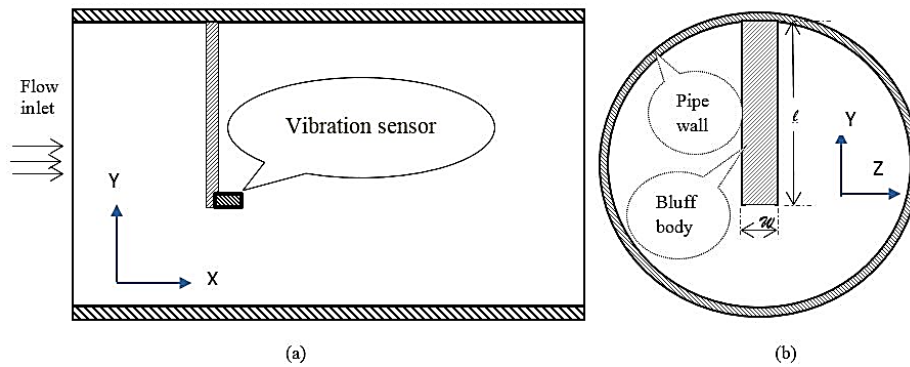


Fig. 4. Line sketch of bluff body with measurement sensor: (a) Front view and (b) Side view.

with the cut off frequency of 800Hz. It was done with a sampling time of 20 sec and 100sec. From the detailed study conducted, they have concluded that a sampling speed of 20 seconds is sufficient for FIV measurement. *Medeiros et al. (2015)* has recorded and analyzed the sampling duration of 20 sec. *Kim and Kim (1996)* has studied the FIV in the frequency range up to 1500 Hz. *Gama et al. (2009)* has studied the vibration levels of U- bend for a test duration of 10 seconds. Based on the studies conducted by various researchers, in this study, in at each flow rate measurements are done for the duration of 30 seconds. Sampling speed used is 3125 samples/second. Since the pumps are isolated from the flow loop used, and the flow is supplied by gravity driven mode, no external noise is expected to add to the signal. So, additional filters are not required to filter out the noise and are not used. In the present study, in each test specimen, twenty five flow rates are measured and are between 2 m³/h to 240 m³/h. Since the loop used can supply the flow of up to 300 m³/h, the measured flow rates are very well within the system specification.

In experimental studies, measurement uncertainty plays a crucial role in its results. In this regard *Usta and Duranay (2021)*, did a detailed uncertainty estimate for a FIV measurement of a circular bluff body in a cross flow. From their analysis, it was found that the uncertainty in measurement is 3.428%. Present study, the set flows are taken from a constant head tank, throughout the test, steady flow rate was maintained which leads to lesser uncertainty. The reference flow meters used are calibrated using the first principle; the expanded measurement uncertainty in flow measurement is less than 0.4%. Additional contributions in measurement uncertainty are from vibration sensor, vibration analyzer and signal conditioner used. The combined uncertainty of flow measurement in this method is 1.85%.

5 RESULTS AND ANALYSIS

5.1 Vortex Shedding Frequency Analysis

This analysis is important to identify the usable flow range of the bluff body used. At first, the drag coefficient and Strouhal number of the bluff bodies are determined. *Tamil Chandran et al. (2022)* has reported the drag coefficient of various samples used

in this study and its Strouhal number was estimated using Eq. 16, which is as given in Table 2.

Table 2 Drag coefficient and Strouhal number

Sample no.	Drag coefficient	Strouhal number
1	1.901	0.1297
2	1.159	0.1880
3	0.842	0.2389
4	1.801	0.1351
5	0.567	0.3214

Natural frequencies of the bluff bodies were determined using exploratory vibration tests and its first natural frequency is reported in Table 3. It was done in immersed condition with a contact type vibration sensor mounted on the bluff body to sense the response. The Strouhal frequencies of the bluff bodies were calculated for the maximum flow velocity of 3.77 m/sec which corresponds to the maximum flow rate used. Details of natural frequency and Strouhal frequency are given in the following Table 3.

Table 3 Natural frequency and Strouhal frequency

Sample no.	Natural frequency in Hz	Max. Strouhal frequency in Hz
1	66.4	48.9
2	74.5	70.8
3	67.5	90.1
4	60.0	50.9
5	61.3	121.2

Since the natural frequency of the bluff body of sample no. 3 & 5, is less than that of the maximum Strouhal frequency, it is expected to have a lock-in effect in these samples at higher flow velocities.

5.2 Flow analysis

Amplitude of vibration generated by a bluff body is proportional to the force acting on it. Natural frequency of the structure will vary based on the

mass loading effect and variation in dynamic stiffness. While increasing the flow velocity, the excitation force is increased proportional to the square of the free stream velocity. Added mass effect generated by the flowing fluid plays a major role in its natural frequency. Based on this concept experimental results are analyzed and presented in three sections. The sections are

Shift in resonance frequency method

- i) Resonance amplitude method
- ii) Overall amplitude estimation method.

Each method used has a unique relationship with the flow rate and FIV. It is discussed in detail in the sections below.

In the resonance amplitude method and overall amplitude estimation method, acceleration amplitude Vs flow rate are plotted. By using a regression model, best fit equations are derived and reported as quadratic/ cubic polynomials. For the derived equation, the variance of the estimated flow with the actual flow is reported as the R-Square value. Where R - square is a statistical measure that represents the propagation of variance between the actual flow rate and estimated flow rate.

In addition to the R – square value, when the best fit line is used for flow estimation, the flow rate indicated at no flow is reported as a zero error.

5.2.1 Flow estimate using shift in resonance frequency method

Basic principle is that the natural frequency of a system depends on its stiffness and mass. When the system is loaded by an additional mass, i.e. added mass by fluid, the natural frequency will be shifted towards the lower side. In addition to the added mass effect of still fluid, researchers have studied the effect of flow velocity in its natural frequency. [Xu *et al.* \(2017\)](#) has studied the effect of flow velocity on natural frequency of bluff body and found that the frequency was reduced due to increase in added mass coefficient, i.e. due to increase in flow velocity. [Khalak and Williamson \(1999\)](#) has studied the change in natural frequency for the velocity ratio (ratio between the flow velocity and natural frequency with diameter/ width of the frontal surface), from 0 to 5.5. From the studies it was observed that there was no appreciable change in frequency up to the velocity ratio of 4.5. Beyond that the frequency was gradually reduced by 6%. Attempts were made by various researchers to use this frequency shift to estimate the flow rate. [Evans *et al.* \(2004\)](#) have studied the change in frequency due to flow rate and observed that it is only in the second decimal. [Dinardo *et al.* \(2013\)](#) also studied the change in frequency and it was observed that it is within 0.1 Hz.

To study the relationship between flow rate and shift in natural frequency, frequency domain plots for one geometrical condition (Sample no. 1) various flow rates were generated. The frequency plot is shown in Fig. 6 (a) and (b). It is plotted in a normalized amplitude scale to demonstrate the frequency shift. As

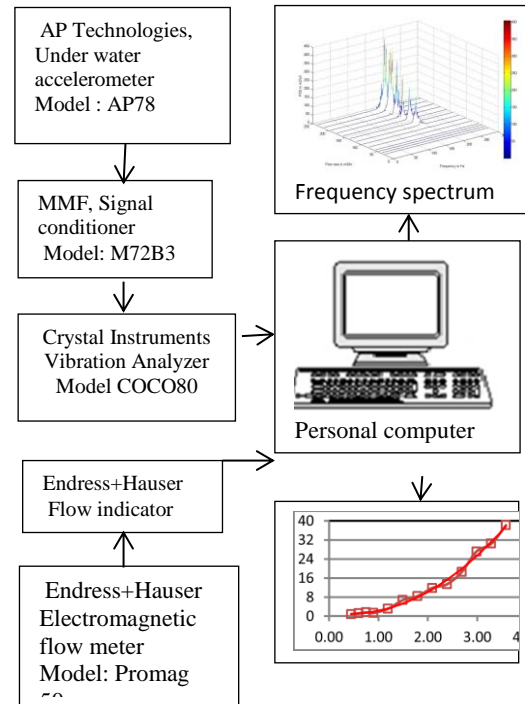


Fig. 5. Data acquisition schematic.

indicated in Fig. 6 (a), at low flow rates i.e. from 2m³/h to 50 m³/h, frequency change was noticed and was in line with the expected range. At the flow rate of 2 m³/h, a resonance frequency of 66.4Hz was observed. While the flow rate was increasing to 20 m³/h, the natural frequency has reduced to 63.2 Hz and with flow rate of 50 m³/h it has further reduced to 57.8 Hz. But with further increase in flow rate, the frequency spectrum widened with more energy content. This is due to an increase in damping, and due to an increase in flow rate. Due to an increase in damping, it makes it difficult to identify the exact shift in frequency vs flow rate as shown in Fig. 6 (b). From the studies conducted it is difficult to implement the flow rate measurement by using frequency shift for higher flow rates. Hence the other two methods are essential to find the correlation with the flow rate.

5.2.2 Flow estimate using resonance amplitude method

When a system is excited by a random source, it will be predominantly excited in its natural frequency. Within the linearity range of the material, the resonance amplitude is proportional to the excitation force. While doing flow measurement studies using FIV, [Evans *et al.* \(2004\)](#), [Dinardo *et al.* \(2013\)](#) also observed that with increase in flow rate, amplitude at the resonance frequency also increased. The resonance acceleration amplitude plots for all the five samples are plotted as acceleration Vs flow rate and are as given in Fig. 7. (a) to (e). In each case the statistical measure of the fitted regression line R² with its best fit line is also plotted and reported.

From the results analyzed, the sample 5 and sample 1 have the R² value of 0.9921, 0.9868 respectively.

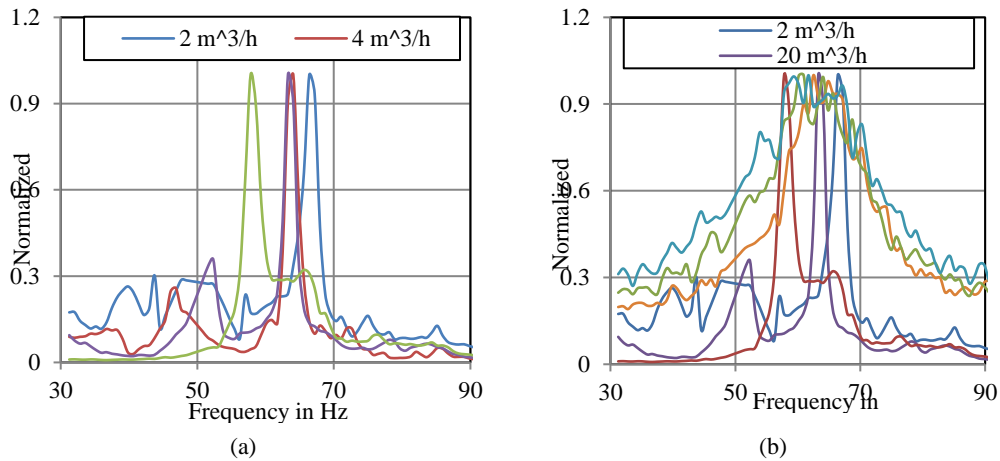


Fig. 6. Normalized acceleration plots; (a) low flow rates, (b) wide range of flow rates

Sample 2, 3 & 4 having the fits drop to 0.9313, 0.9465 and 0.9483 respectively. Deviation in R^2 value in sample 3 is clearly identified from Fig. 7.(c) and (f) . Since the lock-in region of sample 3 is also coming within the measured range, which also leads to a sudden jump in amplitude at that region. In the case of sample 1, it was observed that a well-defined increase in amplitude with respect to increase in velocity is shown in the waterfall diagram Fig. 8. (a). The zero error and R^2 values of the curve fit is as given in Table 4. Sample no. 1 & 5 has a lesser zero error when compared with the other samples. Sample 2 is the highest among the tested samples. Zero error makes the flow measurement less accurate in low flow rates. Other than the zero error, strong correlation between the measured acceleration and flow is found. Fig. 7.(f) , shows the flow Vs amplitude of a combination of all the 5 samples. Again from this plot it is observed that sample no. 3 deviates much from the other samples as expected.

Table 4 R^2 and zero error – Resonance amplitude method

Sample no.	R^2 value	Zero Error in m^3/h
1	0.9868	2.07
2	0.9313	22.34
3	0.9465	12.94
4	0.9483	7.6
5	0.9921	1.66

5.2.3 Flow estimate using overall amplitude estimation method

Other than the above two methods, the overall amplitude estimation method is also used to study the correlation between the vibration levels and the flow rate. The time and Fast Fourier Transform (FFT) data used for the other two analyses are used for this study also. The analysed FFT data has a frequency up to

1600 Hz. From the FFT analysis it is observed that in all the cases, predominant peaks are found below 500 Hz. So for the overall estimation method, only up to 500 Hz is used. Waterfall plot of sample no. 1, 3 is as given in Fig. 8. (a) and (b) respectively. From the waterfall diagrams, it is clear that the predominant FIV is attributed to its natural frequency.

In the overall amplitude method, plots for all the five samples are plotted Vs flow rate and are as given in Fig. 9.(a) to (e). In each case the statistical measure of the fitted regression line R^2 with its best fit line is also plotted and reported. The R^2 values and zero error of the curve fit is as given in Table 5.

Table 5 R^2 and zero error – Overall amplitude estimation method

Sample no.	R^2 value	Zero Error in m^3/h
1	0.995	1.41
2	0.9923	11.55
3	0.9878	12.153
4	0.9915	6.06
5	0.9948	4.05

In this method, the R^2 value of all the samples is above 0.99, indicating a very good correlation between the flow and the overall FIV induced by the flow. In both the resonance amplitude method and overall amplitude estimation method, zero error has a similar trend with slight improvement in the overall amplitude estimation method. Fig. 9.(f) shows the flow Vs overall amplitude of a combination of all the 5 samples. Even though lock-in regions of sample no. 3 & 5 are within the studied range, there is no trend variation observed in this method. Again from this plot it is observed that sample no. 3 deviates much from the other samples. From Fig. 7.(f) and Fig. 9. (f), it is clearly seen that the geometry of the bluff body plays a major role in the FIV correlation.

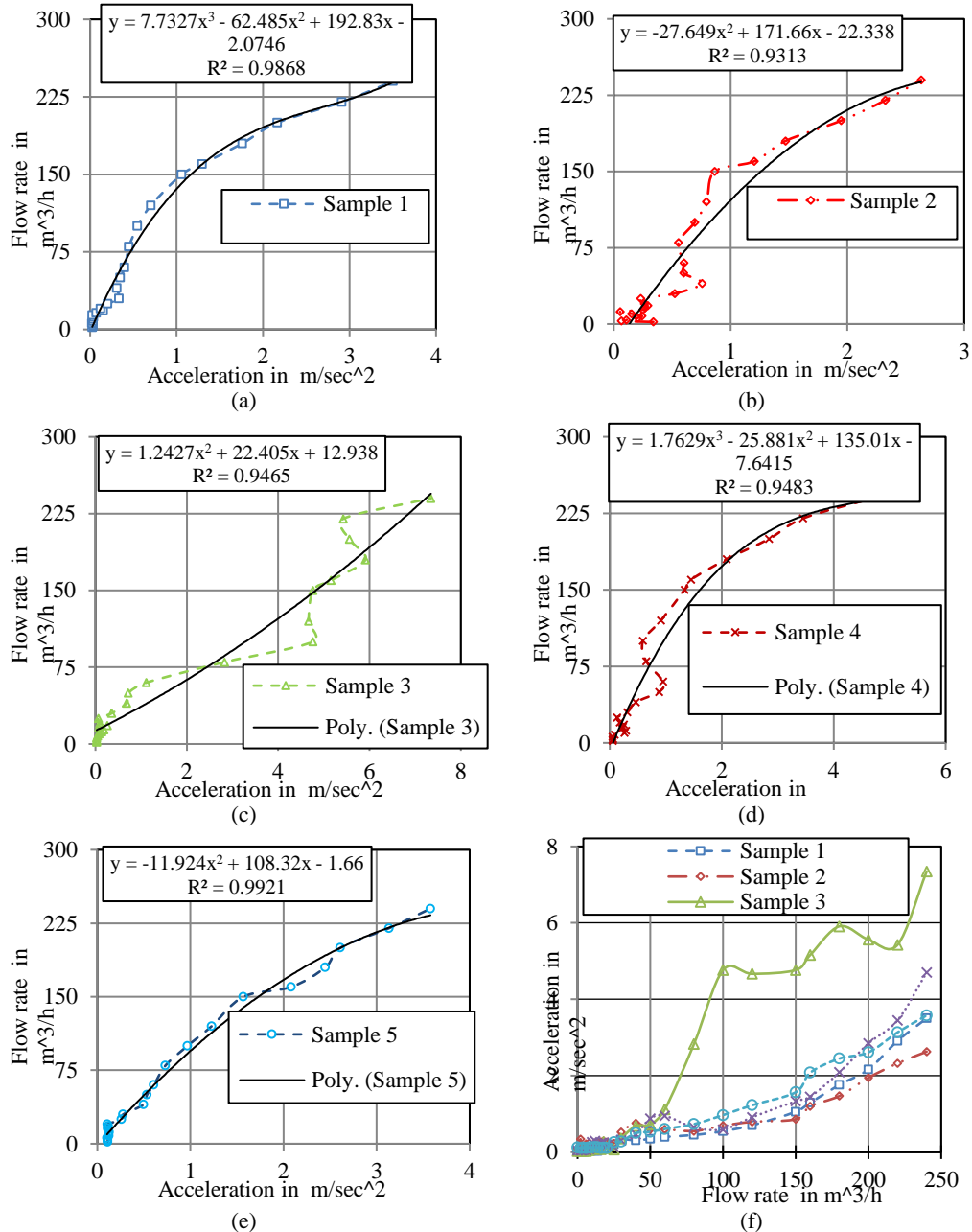


Fig. 7. Acceleration amplitude at resonance frequency Vs flow rate; (a) sample 1, (b) sample 2, (c) sample 3, (d) sample 4, (e) sample 5, (f) sample 1 to 5 (combined).

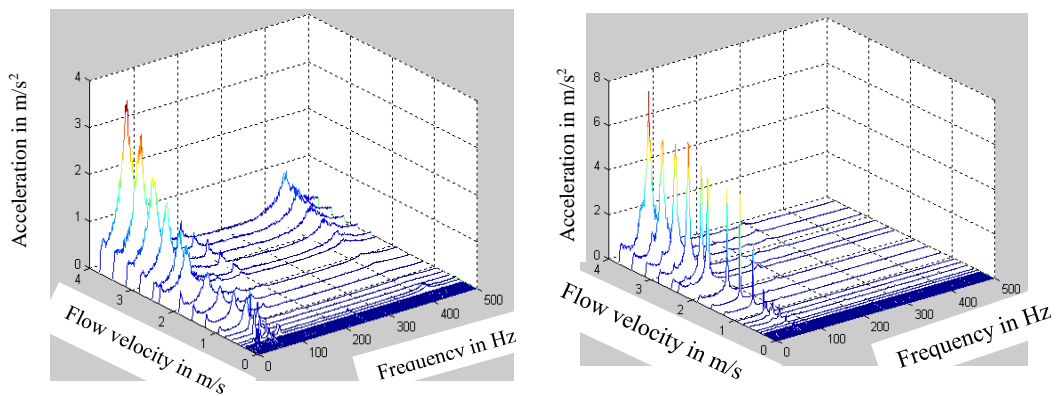


Fig. 8. Waterfall spectrum; (a) sample 1, (b) sample 3.

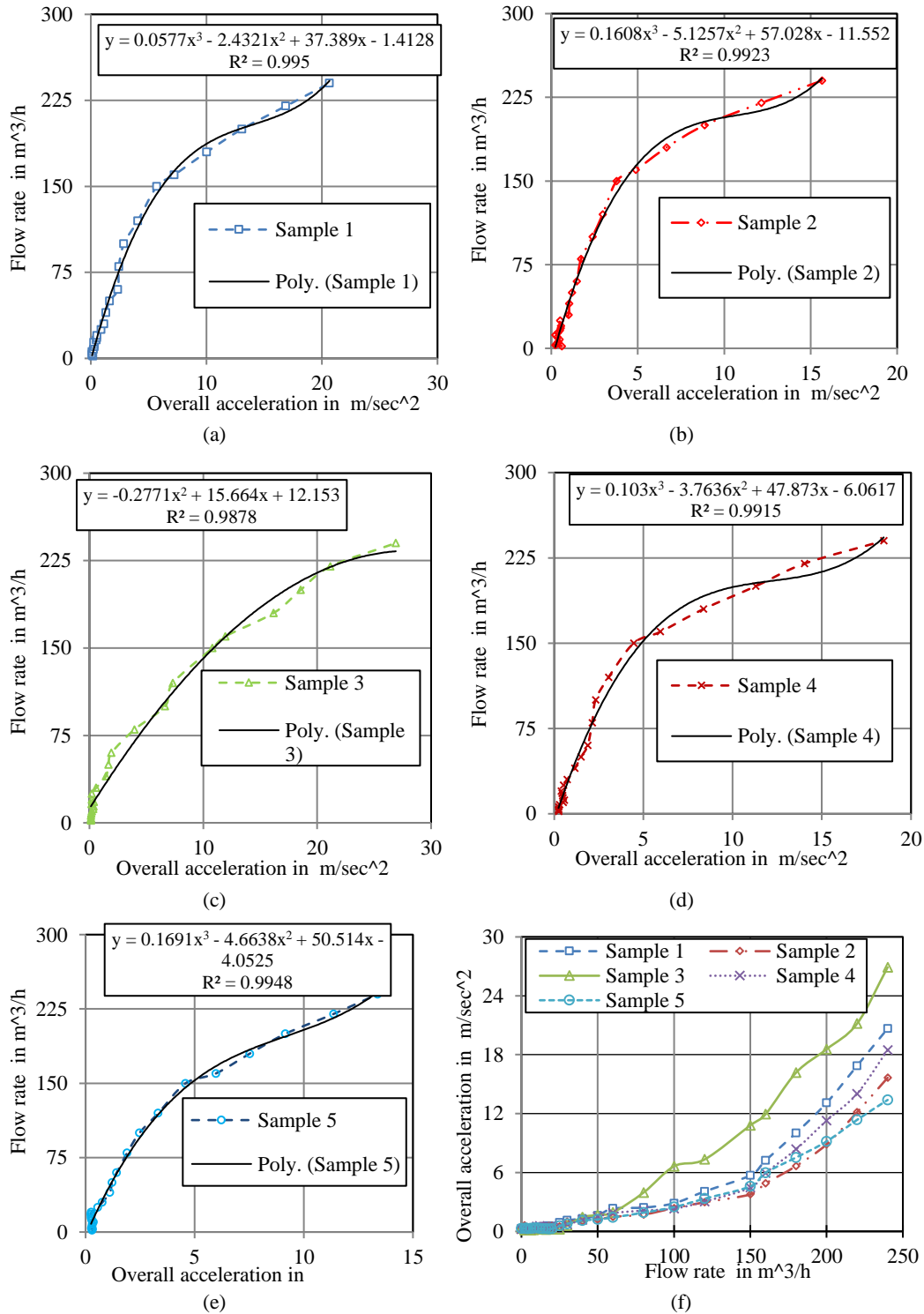


Fig. 9. Overall acceleration Vs flow rate; (a) sample 1, (b) sample 2, (c) sample 3, (d) sample 4, (e) sample 5, (f) sample 1 to 5.

All the above results provides sufficient scope for development of a flow sensor based on the vibration analysis approach presented.

6 CONCLUSION

In summary, it can be concluded that the FIV generated by the bluff bodies have a strong

correlation with the flow passing across it. The curve fit generated shows that it is quadratic/cubic in nature.

For lower flow rates, the frequency shift method shows a linear relation between the flow rate and the bluff body's natural frequency. While increasing the flow rate, the natural frequency of

the bluff body decreases. In the case of a simple cantilever beam it was varying from 66.4Hz at the flow rate of 2 m³/h to 57.8Hz at 50 m³/h. Reduction of 8.6Hz for a flow range of 48 m³/h is a considerable change. The reduction of 0.18 Hz for 1 m³/h gives considerable scope for developing a flow meter using this technique. However the Reynolds number range from 4700 to 5.665x10⁵, this method was correlated only up to Reynolds number of 1.18x10⁵. Beyond that, the peak has widened with increased damping due to increased flow rate. Further, this frequency shift method is ideal at low flows due to very low signal to noise ratio at these flow rates compared to other two methods.

In the Resonance frequency method, shape of the bluff body and vortex shedding frequency plays a major role in resonance amplitude. In semicircular shape, the response was distorted up to the Reynolds number of 3.5x10⁵, which leads to a zero error of 22.34 m³/h, one of the highest of the samples studied. In the case of cylindrical shape, in addition to distortion up to the Reynolds number of 3.5x10⁵, excited by vortex shedding frequency in the upper range of the studied range. This was having a zero error of 12.94 m³/h, which is one of the second highest of the samples studied. Even though the sample of Triangle with semicircular front was excited by vortex shedding frequency, there was no abnormality in its response that was not noticed. This and the simple beam were showing similar behavior with least zero error of near to 2 m³/h and R² value close to 0.99.

In the overall amplitude estimation method, other than sample 3 (Cylindrical shape), other samples have an R² value of above 0.99. Deviation in sample 3 is mainly due to excitation of vortex shedding frequency. In this method, beam (sample no. 1) has the lowest zero error of 1.41 m³/h. Sample 2 & 3 have zero error of more than 10 m³/h. In this method, the influence of vortex shedding in flow measurement is less than the resonance frequency method. This is seen irrespective of geometrical shape.

Combination of using frequency shift method and any one of the other two methods, selected based on geometrical shapes will provide an ideal method for flow measurement using FIV. From the above study, simple beam configuration shows excellent correlation for flow measurement. This configuration can be used in the Reynolds number range of 4700 to 5.655x10⁵ without any difficulties. For use beyond the studied range, the natural frequency of the samples to be increased further so that the vortex shedding frequency is well below it.

ACKNOWLEDGEMENT

The authors would like to acknowledge the support provided by Mr. C. K. Gopan, Senior Research Engineer of M/s Fluid Control Research Institute, for conducting the experimental studies.

REFERENCES

- Belvins, R. D. (1984). *Applied Fluid Dynamics Handbooks*. Van Nostrand reinhand company New York.
- Boiten. W (1993). Flow measuring structures, *Flow Measurement and Instrumentation* 4(1), 17-24.
- Chattopadhyay. P (2006). *Flow meters and flow measurement*. Asian books private limited. New Delhi, India.
- Chen W., S. Wang, X. Shi, C. K. Rheem, Y. Lin and E. Liu, (2022). Numerical simulation of surface roughness effects on the vortex induced vibration of a circular cylinder at a subcritical Reynolds number. *International Journal of Naval Architecture and Ocean Engineering* 14, 100430.
- De Silva, C. W. (2006). *Vibration- Fundamentals and Practice*. CRC Press LLC.
- Dinardo, G., L. Fabbiano and G. Vacca (2013). Fluid flow rate estimation using acceleration sensors. *Seventh International Conference on Sensing Technology (ICST)*. 221-225.
- Evans, R. P., J. D. Blotter and A. G. Stephens (2004). Flow rate measurements using flow-induced pipe vibration, *ASME Journal of Fluids Engineering* 126 (2), 280–285.
- Gama, A., L. Ferreira and P. Filho (2009). Experimental study on the measurement of two phase flow rate using pipe vibration. *Proceedings of COBEM 2009 20th International Congress of Mechanical Engineering*.
- Hoerner, S. F (1965). *Fluid- Dynamic Drag*. Hoerner Fluid Dynamics, Brick town, New Jersey.
- Khalak, A and C. H. K. Williamson (1999). Motions, Forces and Mode Transitions in Vortex-Induced Vibrations at Low Mass-Damping. *Journal of Fluids and Structures* 13 (7–8), 813-851.
- Kim, Y. K and Y. H. Kim (1996). A three accelerometer method for the measurement of flow rate in pipe. *The Journal of the Acoustical Society of America* 100 (2), 717-726.
- Launder, B. E. and D. B. Spalding (1974). The numerical computation of turbulent flows, *Computer Methods in Applied Mechanics and Engineering* (3) 269–289.
- Manzoor, S., J. Khawar and N. A. Sheikh (2013). Vortex-Induced Vibrations of a Square Cylinder with Damped Free-End Conditions, *Advances in Mechanical Engineering* 5 204974.
- Medeiros, K. A. R., C. R. H. Barbosa and E. C. de Oliveira (2015). Flow Measurement by Piezoelectric Accelerometers, *Application in the Oil Industry, Petroleum Science and Technology* 33:13-14, 1402-1409.

- Osman, A. B., M. Ovinis, I. Faye, F. M. Hashim and H. Osei (2018). An Optical Flow Measurement Technique based on Continuous Wavelet Transform, *Journal of Applied Fluid Mechanics* 11(3), 695-707.
- Pittard, M. T (2003). *Large Eddy Simulation Based Turbulent Flow-induced Vibration of Fully Developed Pipe Flow*. Brigham Young University.
- Pittard, M. T. and J. D. Blotter (2003). Numerical Modeling of LES Based Turbulent-Flow Induced Vibration, *ASME International Mechanical Engineering Congress & Exposition*, Washington, 141-148.
- Riverin J. L and M. J. Pettigrew (2007). Vibration Excitation Forces Due to Two-Phase Flow in Piping Elements, *ASME Journal of Pressure Vessel Technology* 129 (1), 7-13.
- Tamil Chandran A., T. Suthakar, K. R. Balasubramanian, S. Rammohan and Jacob Chandapillai (2022). Numerical prediction of the drag coefficient of bluff bodies in three-dimensional pipe flow. *Journal of Computational and Applied Research in Mechanical Engineering* 12 (1) 1-10.
- Tamil Chandran. A., T. Suthakar, K. R. Balasubramanian, S. Rammohan and Jacob Chandapillai (2020). Flow Estimation Using Cross-Flow-Induced Vibration, *Materials, Design, and Manufacturing for Sustainable Environment. Select Proceedings of ICMDMSE 2020, Lecture Notes in Mechanical Engineering*, Springer, Singapore.
- Usta, O and A. Duranay (2021). Uncertainty Analysis of Experiments of Vortex-Induced Vibrations for Circular Cylinders, *Journal of Applied Fluid Mechanics* 14 (2), 541-553.
- White, F. M. (2016). *Fluid Mechanics Eighth edition*, Mc Graw Hill Publication.
- Xinliang, T., M. Chen Ong, J. Yang and D. Myrhaug (2014). Large-eddy simulation of the flow normal to a flat plate including corner effects at a high Reynolds number, *Journal of Fluids and Structures* 49 149–169.
- Xu, Z., B. Jiang and X. Xiao (2017). Instability behaviors of a cylinder array under both increasing and decreasing flow velocities. *Journal of Vibro Engineering* 19 (2), 1393-1408.